Influence of Branching on the Thermal and Crystallization Behavior of Bimodal Polyethylenes Synthesized with Binary Late-Transition-Metal Catalyst Combinations

Ying-Yun Long,[1,2] San-Rong Liu,[1] Lei Cui,[1] Yue-Sheng Li[1]

[1]*State Key Laboratory of Polymer Physics and Chemistry, Changchun Institute of Applied Chemistry, Chinese Academy of Sciences, Changchun 130022, China*
[2]*Graduate School, Chinese Academy of Sciences, Changchun 130022, China*

Received 4 March 2009; accepted 11 August 2009
DOI 10.1002/app.31409
Published online 30 October 2009 in Wiley InterScience (www.interscience.wiley.com).

ABSTRACT: Two reactor blends of linear and branched polyethylene resins with bimodal molecular weight distributions were synthesized in a one-reactor polymerization process through the combination of 2,6-bis[1-(2,6-dimethylphenylimino)pyridyl]cobalt dichloride (**1**) and 2,3-bis(2,6-diisopropylphenyl)butanediimine nickel dibromide (**2**) or 1,2-bis(2,6-diisopropylphenyl)cyclohexene diimine nickel dibromide (**3**) in the presence of modified methylaluminoxane. The linear correlation between the catalyst activity and concentration of the nickel compounds suggested that the catalysts performed independently of one another. The molecular weights, molecular weight distributions, and crystalline and phase structures of the blends were investigated with a combination of high-temperature gel permeation chromatography, differential scanning calorimetry, wide-angle X-ray diffraction, and small-angle X-ray scattering techniques. The branching degree of the polyethylene produced with **3** was much higher than the branching degree of the sample produced with **2**, although their molecular weights were relatively close. In addition, the crystallization rate, melting temperature, degree of crystallinity, and crystallization temperature of more highly branched blends produced with **1**/**3** were lower. The long periods and thickness of the crystalline region were greatly influenced by the addition of highly branched polyethylene. © 2009 Wiley Periodicals, Inc. J Appl Polym Sci 115: 3045–3055, 2010

Key words: blends; crystallization; thermal properties

INTRODUCTION

The blending of two or more polymers is often aimed at controlling the overall properties of the materials. For polyethylene (PE), blending is primarily applied to improve the balance of the processability and mechanical properties of the final product. Different product applications, such as packing and packaging, are closely related to the polymer processing operation and physical properties, which are determined to a great extent by the polymer microstructure. The physical properties of the polymer, such as the stiffness and toughness, are greatly influenced by the molecular weight (MW), molecular weight distribution (MWD), chain branch length, and distribution. High-molecular-weight materials usually exhibit good toughness, but they are inherently difficult to process because of their high melt viscosities. This shortcoming can be overcome with processing aids, but this solution is costly. Therefore, for important industrial applications, the blending of PEs with different MWs, MWDs, chain branch lengths, and distributions is often employed to overcome this imbalance. Our study was initiated to investigate and further develop our understanding of the structure–property relationship in bimodal resins.

These structural features of PE can be controlled during the original polymerization process and depend on the catalyst type and the reaction conditions. Considerable efforts have been made to improve the polymerization techniques and the choice of catalyst combinations. Up to now, there have been four major methods used to obtain polyolefin blends with different shortcomings and advantages.[1–5] The first method is the postpolymerization mixing of different polymers in a extruder under the proper conditions; this has problems of energy consumption, operational costs, and miscibility limitations. The second method involves multiple reactors (tandem or cascade reactor systems) generating different polymers through the variation of the reaction conditions in each reactor. This method, used at the pilot plant level, has been revealed to be expensive and time-consuming. The third method depends on the variation of operation conditions, such as the

Correspondence to: Y.-S. Li (ysli@ciac.jl.cn).
Contract grant sponsor: National Natural Science Foundation of China; contract grant number: 50873097.
Contract grant sponsor: Special Funds for Major State Basis Research Projects (Ministry of Science and Technology of China); contract grant number: 2005CB623800.
Journal of Applied Polymer Science, Vol. 115, 3045–3055 (2010)

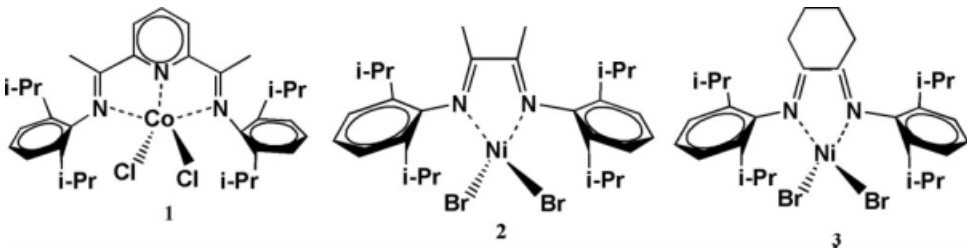

Scheme 1 Structures of catalysts **1**, **2**, and **3**.

temperature and ratio of hydrogen and monomer pressures, in a single reactor. Here, two sets of polymerization catalyst combinations were employed within a single reactor to produce bimodal polymer resins; this is the fourth method. The key to designing blends with the required microstructures by this method is the choice of the proper combination of catalysts that can produce polyolefins with different properties independently. The selected catalysts will be based on the polymer performance desired and the special characteristics of families of olefin polymerization catalysts. In this way, the ideal reactor blends can be adjusted by simple variations of the catalyst ratio and polymerization conditions. This method has received considerable attention by industrial laboratories, as can be seen by the number of patents issued in recent years.[6–10]

Many researchers have devoted themselves to exploring and studying better catalyst combinations for producing bimodal or broader PEs.[4,5,11–18] Several studies have shown that ethylene polymerizations with combinations of different catalysts and variations of the polymerization processes can produce reactor blends with improved physical and/or chemical properties.[1,4,5,11–13,19–22] In most of the early reports, metallocene catalysts such as titanium, zirconium, and hafnium compounds were the main choices for catalyst combinations.[11,23,24] Some catalysts combined in a polymerization reactor have been successful in producing ethylene homopolymer independently,[5,15–17] and this suggests that the active sites are not affected by interactions between the different site types present in the polymerization mixtures. Depending on the binary system, variability of the MWD and catalytic activity can be achieved. Moreover, Soares and coworkers[25,26] reported their mathematical modeling of polymerization using metallocene compound combinations based on experiments to predict polymerization conditions that will produce desired PE resins. That team also investigated the relationship between the composition of resins and their physical properties.[4,13] Wu et al.[27] studied the crystalline structure and phase structure of metallocene linear low-density PE and low-density PE blends, and they found that both a cocrystallization phenomenon and phase separation existed. In addition, Mandelkern et al.[28] reported that the extent of cocrystallization of blends with different types of PE was governed by the closeness of the crystallization rates of each component. However, most of the reported blends were obtained through the mixing of the two species involved and could not be uniformly blended by one-reactor polymerization.

Recently, we investigated the effect of combining late-transition-metal catalysts in different ratios on blend microstructures and physical properties.[5] We have improved the balance of processability and physical properties. The focus of this report is the influence of the MW and degree of chain branching on the thermal and crystalline behavior of the resins. Here, late-transition-metal catalysts were used to produce wide-MWD PE blends with low-MW linear polyethylene (LPE) and higher MW, more or less highly branched polyethylene (HBPE) in different feed ratios. The three catalysts shown in Scheme 1 are 2,6-bis[1-(2,6-dimethyphenylimino)pyridyl]cobalt dichloride (**1**), which is known as an active catalyst for producing LPEs with low MWs that are less affected by the polymerization conditions,[29–31] and 2,3-bis(2,6-diisopropylphenyl)butanediimine nickel dibromide (**2**) and 1,2-bis(2,6-diisopropylphenyl) cyclohexene diimine nickel dibromide (**3**), which are both active for producing branched PEs with higher MWs without any other comonomer.[32–36] Although only the nickel compound is substituted in combinations compared with previous work,[5] we have found some different results with respect to the branching degree, thickness of the lamellar crystallinity, and crystallization rate.

EXPERIMENTAL

Materials

Anhydrous toluene was purified with a solvent purification system purchased from Mbraun (Garching, Germany). Modified methylaluminoxane (MMAO; 7% aluminum in a heptane solution) was purchased from Akzo Nobel Specialty Chemical, Inc. Ltd. (Shanghai of China). Catalysts **1–3** were synthesized according to procedures reported in the literature.[29–32]

Typical polymerization procedure

Polymerizations were carried out in a 1-L stainless steel reactor equipped with a mechanical stirrer and internal cooling water coils. The reactor was baked under a nitrogen flow for 12 h at 150°C, subsequently cooled to the desired reaction temperature, and then purged by ethylene three times. The prescribed amounts of each catalyst solution (**1** and **2** or **1** and **3**) and toluene were injected simultaneously into the reactor via a gastight syringe. Ethylene was introduced into the reactor, and the pressure was maintained at 5 atm throughout the polymerization run by the continuous feeding of ethylene gas. After the polymerization had proceeded for 30 min, we stopped it by turning the ethylene off and relieving the pressure. The reaction mixture was poured into a solution of HCl and ethanol (10 vol %). The polymer was isolated by filtration, washed with ethanol, and dried *in vacuo* at 60°C for 24 h.

Polymer Characterization

The MWs and MWDs of the samples were determined at 150°C with a PL-GPC 220 high-temperature gel permeation chromatograph (Polymer Laboratory, UK) equipped with three PL-gel 10-μm mixed-BLS type columns; 1,2,4-trichlorobenzene was employed as the solvent at a flow rate of 1.0 mL/min. The calibration was made with the EasiCal PS-1 polystyrene standard (PL, Ltd., UK). The MW and MWD values were obtained with a polystyrene standard for these PE blends with different degrees of branching. The degree of branching of the branched PE obtained from the pure nickel complex was determined by quantitative ^{13}C-NMR spectroscopy. The measurement was performed at 120°C on a Varian Unity 400 (Bruker, Switzerland) with *o*-dichlorobenzene as the solvent. Differential scanning calorimetry (DSC) measurements were performed on a PerkinElmer (USA) Pyris 1 DSC instrument under an N_2 atmosphere. The samples were heated from 0 to 150°C and cooled to 0°C at a rate of 10°C/min. The melting temperature (T_m) and heat of fusion (ΔH_f) were taken from the second heating curve. The DSC-determined degree of crystallinity (X_C^{DSC}) was calculated from ΔH_f with eq. (1):[37]

$$X_C^{DSC} = \Delta H_f / \Delta H_{f(\text{standard})} \quad (1)$$

where $\Delta H_{f(\text{standard})}$ is the heat of fusion for the linear polyethylene with 100% crystallinity, which is about 289 J/g. [5]

The same instrument was used to study the isothermal crystallization kinetics of the blends. The samples were heated to 150°C and held there for 3 min, then quickly cooled to the designed isothermal temperature, and then held for 30 min. The exothermic curves of heat flow as a function of time were recorded and investigated. Wide-angle X-ray diffraction (WAXD) patterns were recorded in the reflection mode at room temperature with a D/MAX 2500V connected to a computer (Philips, Amsterdam, Netherlands). The samples were pressed into 1-mm-thick plates at 30–50°C above T_m. The diffraction scans were collected over a period of 20 min from 5 to 40° with a sampling rate of 1 Hz. The WAXD-determined degrees of crystallinity ($W_{C,X}$ or X_C^{WAXD}) of the PE blends were calculated with eq. (2), which was developed by Yin and Mo:[37]

$$W_{C,X} = \frac{I_{110} + 1.42I_{200}}{I_{110} + 1.42I_{200} + 0.68I_a} \quad (2)$$

where I_{110} and I_{200} are the intensity of the two major crystalline peaks at scattering angles of about 21.46° and 23.70° in the WAXD profiles (Fig. 8), separately; I_a is the intensity of the amorphous peak at scattering angle of 19.5° in the WAXD profiles (Fig. 8). We can learn the details from Yin and Mo.[37]

Small-angle X-ray scattering (SAXS) measurements were performed on a Philips PW-1700 diffractometer (Anton Paar, Austria), connected to a Krathy compact system (Anton Paar, Austria), which was operated at 40 kV and 30 mA with a 0.5° step size from 0.08 to 3.0° (2θ). The absolute intensity for $I(S)$ (the ratio of the test sample's scattering intensity from experiments and the absolute intensity of a standard sample) was evaluated with a four-slit collimation system, and the mensuration of the absolute intensity was carried out on standard samples.

RESULTS AND DISCUSSION

Choice of the catalyst combination

As we have mentioned previously, the catalysts should polymerize ethylene independently, and the pure polymer can be obtained under certain conditions. We expected to get blends of a low-MW polymer with a linear structure and a high-MW polymer with a high branching degree in different ratios. On the basis of our previous work,[5] we changed the catalyst 1,4-bis(2,6-diisopropylphenyl)acenaphthene diimine nickel dibromide, which can polymerize ethylene to produce HBPEs with high MWs, to **2** or **3**, with which we can get less highly branched but much higher MW PEs or more highly branched and higher MW PEs in comparison with the previously obtained HBPE.[5]

The ethylene polymerizations were carried out with different ratios of the catalyst fractions at 5 atm. In this study, two sets of resins were produced. Each set contained a pure low MW linear PE, a pure HBPE, and some blends with different HBPE contents. Set A consisted of samples produced with

TABLE I
Ethylene Polymerization with the Binary Catalytic Systems 1,2/MMAO and 1,3/MMAO

Sample	X_{Ni} (%)[b]	Activity (kg of PE/mol of Co + Ni h)	M_w (kg/mol)[c]	Polydispersity index[c]	W_{tHBPE} (%)	T_m (°C)[d]	T_c (°C)[d]	ΔH_m (J/g)[d]	X_C[d]	X_C[e]
A1[a]	0	3.77	21	2.6	0	133.6	117.8	217.7	0.76	0.77
A2	30.0	2.89	97	8.3	13.8	131.7	116.9	187.4	0.66	0.66
A3	35.0	2.65	119	9.2	17.9	131.1	116.2	168.3	0.59	0.59
A4	50.0	2.10	141	12	28.5	130.9	115.3	140.0	0.49	0.50
A5	65.0	2.01	210	15	42.8	130.7	114.6	92.6	0.32	0.33
A6	75.0	1.85	374	16	54.8	130.0	114.0	38.2	0.13	0.13
						127.1	108.1			
A7	86.0	1.80	399	10	71.0	125.0	105.1	33.9	0.12	0.12
						119.0	56.9			
A8	90.0	1.76	504	19	78.7	120.5	101.4	19.1	0.06	0.07
A9	96.0	1.71	549	20	90.5	116.6	96.9	2.81	0.01	0.01
A10	100.0	1.52	607	2.3	100	—	—	—	—	—
B1[f]	0	1.86	25	2.0	0	131.0	114.8	185.9	0.64	0.65
B2	25.0	1.62	105	8.9	14.9	130.4	114.2.	158.9	0.55	0.55
B3	35.0	1.55	165	8.7	22.1	129.5	113.9	98.4	0.34	0.35
B4	50.0	1.47	223	15	34.5	128.8	110.9	78.3	0.27	0.28
B5	60.0	1.37	285	15	44.1	128.1	110.2	65.2	0.22	0.22
						125.2	108.9			
B6	75.0	1.25	335	13	61.2	127.5	97.2	22.9	0.08	0.09
						126.8	82.2			
B7	85.0	1.15	403	7.6	74.9	126.5	94.0	7.05	0.02	0.03
B8	100.0	0.98	506	1.9	100	—	—	—	—	—

[a] These samples were synthesized under the following reaction conditions: solvent = toluene (500 mL), temperature = 30°C, n_{Co+Ni} = 20 μmol, Al/M = 1500, and ethylene pressure = 10 bar.
[b] X_{Ni} = moles of **2** or **3**/(moles of **1** + moles of **2** or **3**).
[c] Determined by high-temperature gel permeation chromatography.
[d] Determined by DSC.
[e] Determined by WAXD.
[f] These samples were synthesized under the following reaction conditions: solvent = toluene (500 mL), temperature = 30°C, n_{Co+Ni} = 30 μmol, and Al/M = 1500, and ethylene pressure = 5 bar.

1,2/MMAO, and set B consisted of samples produced with **1,3**/MMAO. The typical polymerization results are listed in Table I. As shown in this table, we found that not only the catalytic activities but also the MW, MWD, T_m, crystallization temperatures (T_c), and degree of crystallinity (X_C) values of the PE blends varied with the molar fraction of catalyst **2** or **3** (X_{Ni}). The pure HBPEs produced with catalysts **2** and **3** displayed the highest (605 kg/mol) and second highest MWs (506 kg/mol), respectively, whereas the LLPE produced with catalyst **1** showed the lowest MWs (22 kg/mol for A1 and 25 kg/mol for B1). Both the MWs and MWDs can be adjusted in the ranges of 22–605 kg/mol and 2.1–20, respectively, for set A and in the ranges of 25–506 kg/mol and 1.9–15, respectively, for set B by the variation of the catalyst ratios.

The relationship between the catalytic activities and X_{Ni} is presented in Figure 1. Obviously, the catalytic activities of **1** and **2** were much higher than those of **1** and **3** under different polymerization conditions. For set A, catalysts **1** and **2** showed the highest and lowest catalytic activities under the same polymerization conditions, respectively. The catalytic activity decreased linearly with the increase in X_{Ni} in the reaction medium, and this was similar to the case of set B. This linear correlation between the catalytic activity and X_{Ni} implied that interactions between species **1** and **2** or **3** were minimal, and the

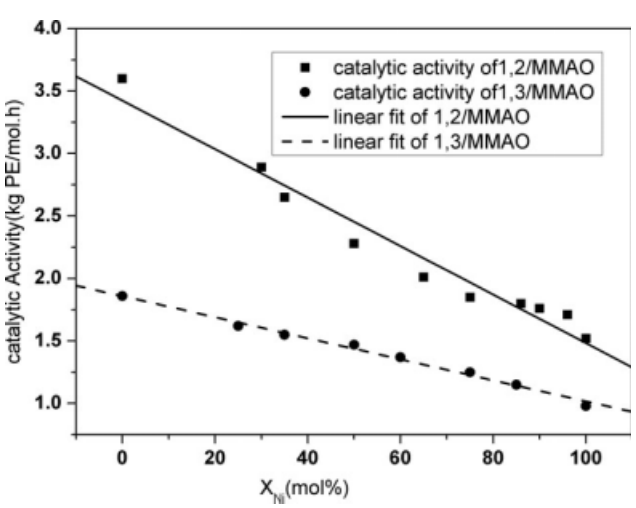

Figure 1 Relationship between the percentage of catalyst **2** or **3** and the catalytic activity.

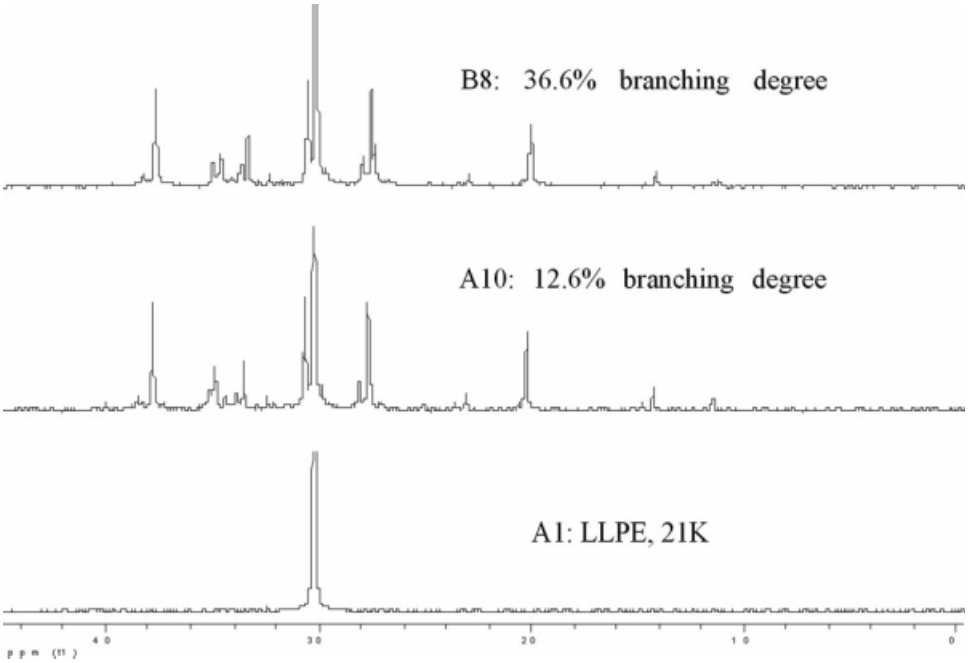

Figure 2 ^{13}C-NMR spectra of LPE (A1) and HBPE (A10 and B8) obtained from catalysts **1**, **2**, and **3**.

catalysts performed independently; this is similar to the results in other reports.[5,15–17]

Microstructural characterization

The degree of branching is one of the most important molecular parameters of PE resins because it characterizes the difference in the molecular structure with respect to their linear analogue. Figure 2 shows quantitative ^{13}C-NMR spectra of A1, A10, and B8. The branching degree of PE was calculated according to the rules of Galland and Qiujada.[38–40] It is remarkable that there were plenty of side branches, including some short branches (methyl, ethyl, butyl, and amyl) and long ones ($n \geq 6$), in traces of A10 and B8, whereas the trace of A1 showed no side branches (Fig. 2). The results of the analysis of the branch structures of A10 and B8 are listed in Table II. It is noteworthy that the long branches confirmed by the peaks at 29.98 and 32.39 ppm for trace A10 were much more numerous than the short chains, except for methyl. However, the trace for B8 showed that the long branch content was not only much less than the methyl branch content but also less than the contents of ethyl, butyl, and amyl branches. On the other hand, the total branching degree of B8 was 36.6%, which was much higher than the degree of A10 (12.6%). In addition, the branching degrees of all blend samples determined by ^{13}C-NMR were almost the same as the calculated data according to the weight percentage of HBPE, which also proved that the catalysts performed independently of one another.

Figure 3(a,b) shows the bimodal MWDs of the blends for set A and set B, respectively. These pictures reveal that such binary catalyst combinations can produce broad and bimodal PE blends with different MWs in a single reactor by the alteration of the catalyst ratios under certain conditions. We also found a little excursion of the peaks for the MW of the blends near the peak values of pure PEs, and this may be linked to the difficulties encountered in the polymerization process, which was free from defects. To further study the compositions of the

TABLE II
^{13}C-NMR Analysis of HBPE Synthesized with Catalysts 2 and 3

	Branch content[a]		Percentage over total branching		Percentage of branching	
Branch type	A10[b]	B8[b]	A10	B8	A10	B8
N_{methyl}	18.61	1.524	55.8	56.0	7.03	20.48
N_{ethyl}	2.57	0.274	7.70	10.1	0.97	3.69
N_{propyl}	ND	0.056	—	2.0	—	0.75
N_{butyl}	1.00	0.332	2.94	12.2	0.37	4.45
N_{amyl}	2.66	0.328	7.93	12.0	1.00	4.40
N_{long}	8.54	0.217	25.63	7.7	3.23	2.79

ND = not determined (i.e., below the qualification limit).

[a] The values were obtained via calculations using the integral areas of each related peak according to ref. 40. Different peaks in the two ^{13}C-NMR spectra were chosen as standard peaks, and this led to different absolute branch contents.

[b] A10 and B8 correspond to the polymers produced with catalysts **2** and **3**, respectively.

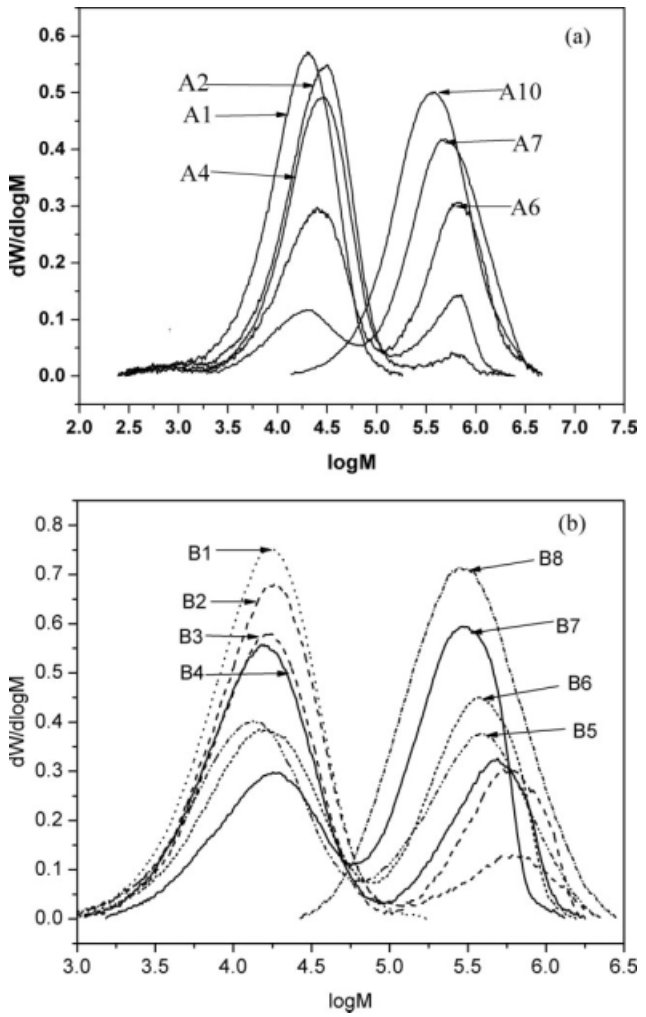

Figure 3 MWDs of the blends obtained with the binary catalysts. M is the molecular weight of a certain samples and W is the weight of such samples with molecular weight of M.

blends, linear superpositioning of two Flory–Stockmayer distributions was used to test the proportions of the weight of HBPE of each sample. The MWD of sample A3 and the associated fit are presented in the top right of Figure 4. The tags A1 and A2 in this picture mean the areas of the spectroscope associated with LPE and HBPE obtained with catalysts **1** and **2** of the reactor blends, respectively. Moreover, the ratio of the two areas was equal to the weight ratio of LPE to HBPE in the blends. Consequently, with this method, we could obtain the relationship between the weight ratio of LPE to HBPE and X_{Ni}. The results related to the blends of set A are shown in Figure 4, and the details for set B are displayed in Table I. This means that we can design PE blends with appropriate MWs according to this picture.

Figures 5 and 6 show the results of DSC measurements for all the samples of set A. No obvious crystallization or melting peak was observed for sample A10, and this proves that it had an amorphous

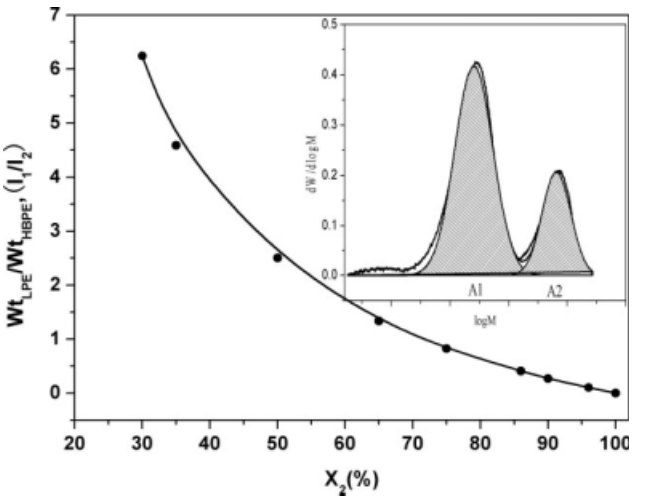

Figure 4 Plot of LPE versus HBPE in the blends of set A and the associated fit of bimodal sample A3 via two Flory–Stockmayer distributions.

structure and a high degree of branching. It is very interesting to find broad or double melting endotherms for samples A5–A9 in the melting traces. All the melting and crystallization peaks shifted toward lower temperatures and became wider with increasing HBPE content in the blends. For the samples of set B, similar behaviors were found. The only difference existed in the lower T_m and T_c values in comparison with those of set A, which are clearly displayed in Table I. Such phenomena were discovered and explained clearly for similar systems in earlier reports[5,41–45] and were predominantly due to the different increased contents of HBPE in the mixtures.

Figure 7 presents the relationship between the weight content of HBPE in the blends (W_{tHBPE}) and X_C. The two horizontal lines depict the constant values of X_C, indicating incompatible blends. For the

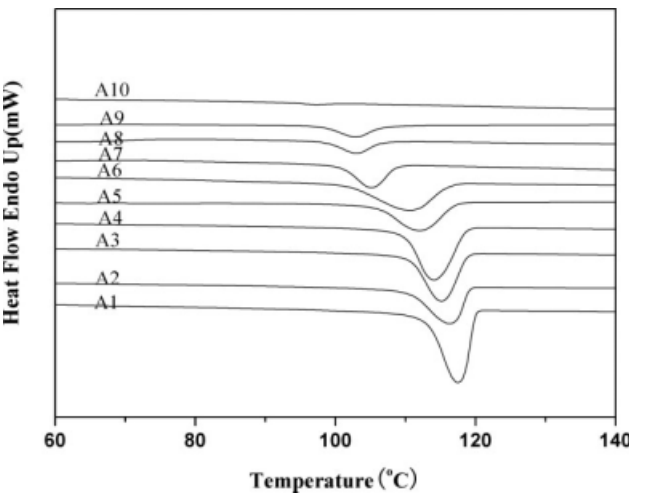

Figure 5 Effect of the HBPE content on the T_c values of all PE samples of set A.

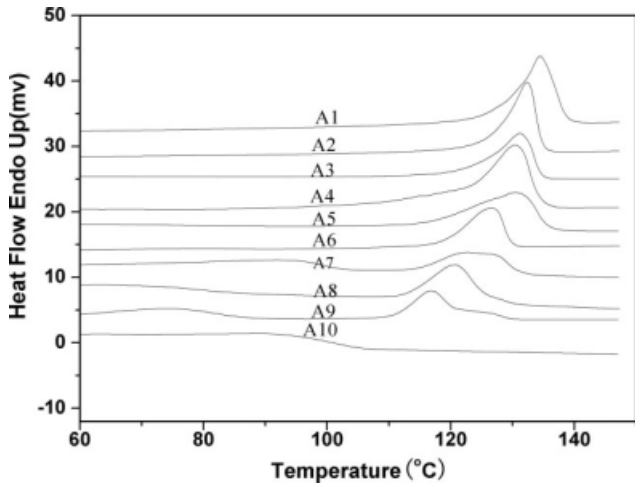

Figure 6 Effect of the HBPE content on the T_m values of all samples of set A.

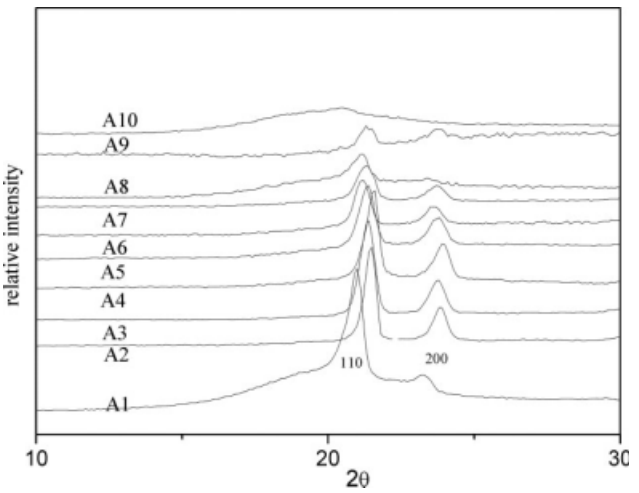

Figure 8 X-ray diffractograms of all PE samples of set A.

blends studied here, there are evidently decreasing curves, and all the data points are below the horizontal lines; this signifies that such PE mixtures are compatible systems and that the addition of HBPE slows their crystallization process in comparison with the pure LPE synthesized with catalyst **1**. The constant value of X_C for A1 was higher than that for B1 because of the lower MW and higher initial X_C value. Moreover, the decreasing slope for the blends of set A was greater than that for set B because of their lower branching degree.

To further investigate whether or not the addition of HBPE affects the formation of crystals during crystallization and the amount of crystalline content formed, a WAXD experiment was conducted. Ordinarily, LPE has its typical orthorhombic lattice in crystallization, and the diffractograms exhibit two major crystalline peaks at scattering angles of $2\theta = 21.46 \pm 0.10^\circ$ and $2\theta = 23.70 \pm 0.10^\circ$, which correspond to the reflection planes at 110 and 200, respectively.[37] The clear and identical peak positions from the WAXD profiles for the samples of set A are displayed in Figure 8; these are the same as the profiles for the samples of set B and our reported blend system.[5] Obviously, the characteristic orthorhombic crystals were retained, and the structure of LPE was not influenced. However, the intensity decreased with the increasing content of HBPE in all samples because the consecutive ethylene units decreased and the crystallizable components became smaller as the proportion of HBPE increased in the blends. According to eq. (2), we could obtain the X_C^{WAXD} values of the blends as listed in Table I. It also proved that the reduction of X_C could be attributed to the increasing HBPE content of the PE blends.[46]

SAXS measurements were performed to study the perspicuous structure of such a two-phase system comprising crystalline and amorphous fractions of

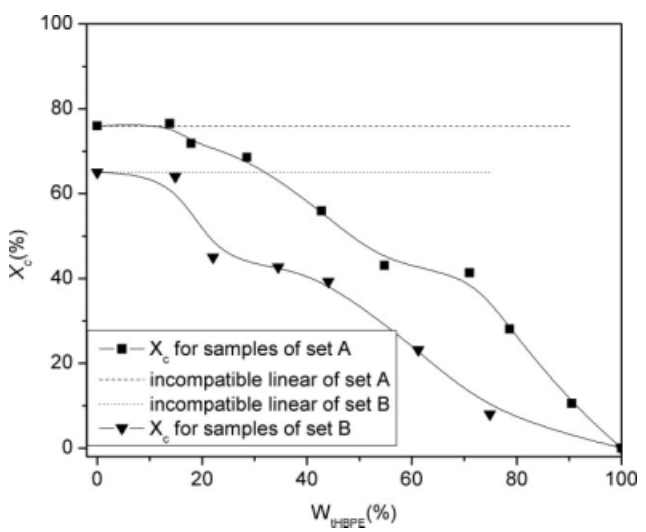

Figure 7 Effect of $W_{t\text{HBPE}}$ on X_C of the blends of set A.

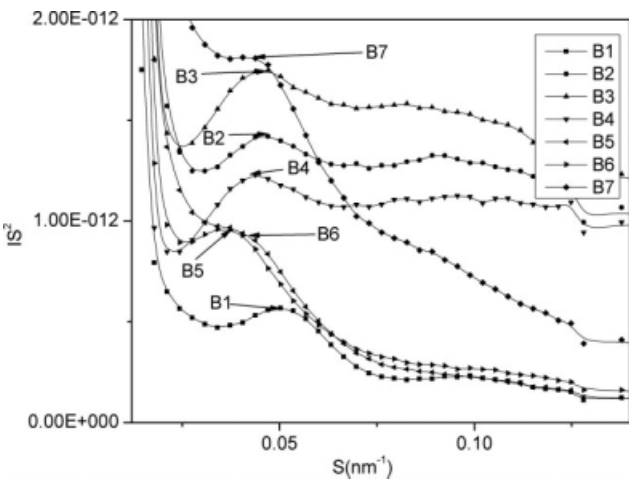

Figure 9 Lorentz-corrected SAXS profiles for the PE blends of set B. $S = 2\sin\theta/\lambda$. θ is the Bragg angle, λ is the wavelength of X-ray, I is the scattering intensity after defuzzification.

TABLE III
L_B and L_C Values for the Samples

	Sample[a]									
	1	2	3	4	5	6	7	8	9	10
$W_{t\text{HBPE}}$ (%)[b]	0	13.8	17.9	28.5	42.8	54.8	71.0	78.7	90.5	100
S (nm^{-1})[c]	0.0486	0.0437	0.0408	0.0391	0.0366	0.0376	0.0420	0.0437	0.0477	—[g]
X_C^{WAXDb}	0.77	0.66	0.59	0.50	0.33	0.13	0.12	0.07	0.01	0
L_B (nm)[b]	20.57	22.88	24.52	25.61	27.32	26.58	23.83	22.86	20.95	—
L_C (nm)[b]	15.84	15.10	14.47	12.81	9.02	3.46	2.86	1.60	0.21	—
$W_{t\text{HBPE}}$ (%)[d]	0	14.9	22.1	34.5	44.1	61.2	74.9	100	—[f]	—[f]
S (nm^{-1})[e]	0.0504	0.0469	0.0450	0.0438	0.0375	0.0369	0.0431	—[g]	—	—
X_C^{WAXDd}	0.65	0.55	0.35	0.28	0.22	0.09	0.02	0	—	—
L_B (nm)[d]	19.85	21.32	22.20	22.85	26.68	27.14	23.16	—	—	—
L_C (nm)[d]	12.90	11.73	7.77	6.40	5.87	2.44	0.47	—	—	—

[a] The sample number for set A or B.
[b] Parameter for set A.
[g] Value of S for set A ($q_{\max} = 2\Pi \times S$).
[d] Parameter for set B.
[e] Value of S for set B ($q_{\max} = 2\Pi \times S$).
[f] No sample for set B.
[g] No values of S were obtained from Lorentz-corrected SAXS profiles for amorphous samples A10 and B8.

the PE blends. The Lorentz-corrected SAXS scattering profiles in absolute intensity units for samples of set B are presented in Figure 9. The observed reflection peaks in Figure 9 are the first- and second-order reflections corresponding to the lamellar structure. On the basis of the maximum value of the scattering vector ($q_{\max}$) observed in the Lorentz-corrected SAXS scattering profiles and Bragg's law, the mean long period of the lamellar morphology could be calculated with the following equations:[37,46,47]

$$L_B = \frac{2\pi}{q_{\max}} \tag{3}$$

$$q = \frac{4\pi \sin(\theta/2)}{\lambda} \tag{4}$$

where q is the scattering vector and λ is the wavelength. The long period (L_B) is composed of the crystal region (L_C) and the amorphous region (L_A) in an alternating fashion in the lamella. L_C can also be estimated with eq. (5):

$$L_C = L_B X_C^{\text{WAXD}} \tag{5}$$

The structural parameters obtained by SAXS measurement are summarized in Table III. As shown in Figure 10, L_B first increased slightly with the increase in the HBPE content in the blends for both sets and then presented a gradually decreasing tendency when $W_{t\text{HBPE}}$ was over approximately 50%; this was somewhat different from the decreasing tendency of Wu et al.'s system.[27] We can assume that the addition of amorphous HBPE to our system led to increasing L_A values because of its much higher MW in comparison with the low-density PE that they used. In contrast, the L_C values monotonously decreased with increasing HBPE content because of the syncretization of the HBPE component with the amorphous region of the original LPE, and this accorded with their results.[27] Figure 10 shows that the L_B values were inclined to decrease at higher HBPE concentrations, indicating that the amorphous region and crystalline region could be rearranged after being destroyed; this was similar to the findings of the early reports.[21,27,28,45]

To assess the nature of the crystallites that developed and evaluate the impact of the temperature on the crystallization process, isotherm crystallizations were performed with the obtained PE samples. Initially, the samples were held in a melted condition at 150°C for 3 min, and then they were quickly cooled to T_c at the rate of 80°C/min and were maintained for

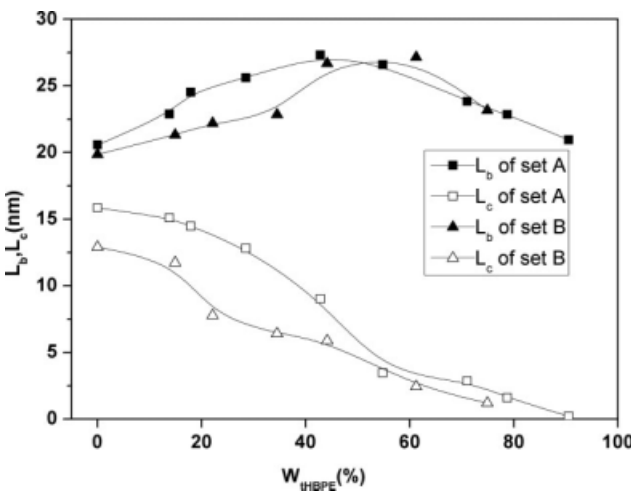

Figure 10 Plots of L_B and L_C of the blends versus $W_{t\text{HBPE}}$.

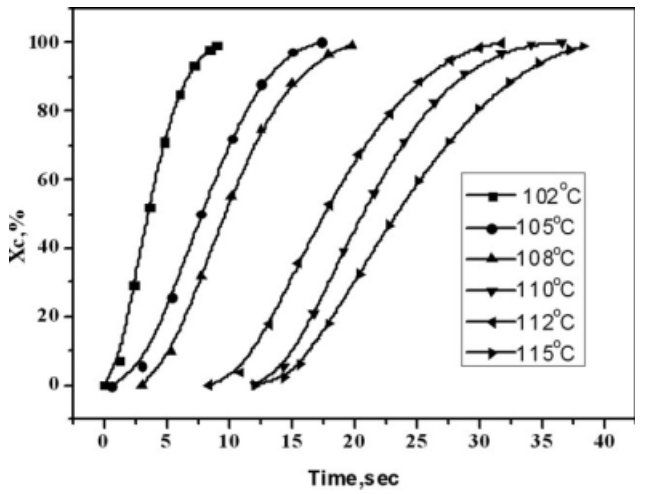

Figure 11 Crystallization isotherms of sample A3 crystallized at different T_c's.

30 min at each T_c. With the following Avrami equations, we could analyze the bulk kinetics of the isothermal crystallization of the blends:

$$\log[-ln(1 - X_C)] = \log K + n \log t \quad (6)$$

$$K = \ln\left(\frac{2}{t_{1/2}^n}\right) \quad (7)$$

where t is the time, n is the Avrami exponent related to the geometry of spherical growth and the mechanism of nucleation, K is the total kinetic rate constant, and $t_{1/2}$ is the time required to reach 50% relative crystallization (i.e., the half-time of crystallization).

The typical crystallization isotherms for sample A3 shown in Figure 11 were obtained from plots of X_C versus time at different T_c's. With this series of curves and eq. (7), the value of $t_{1/2}$ could be calculated, and the fact that $t_{1/2}$ increased with increasing temperature was obvious, as shown in Figure 12. Additionally, the increasing rates of $t_{1/2}$ were different at various temperatures and with diverse HBPE contents for the PE blends. Furthermore, the crystallization rate decreased with increasing T_c and a greater amorphous component (HBPE) concentration in the blends. Such descriptions also fit the blends in set B. However, the crystallization rate decreased faster with the same HBPE content because of the much higher branching degree and MW of B8. In other words, the addition of the amorphous component did not disturb the crystallization process of LPE. In addition, such crystallization isotherm experiments can afford some important information about miscibility and polymer–polymer interactions on the basis of the results calculated with the following equation:

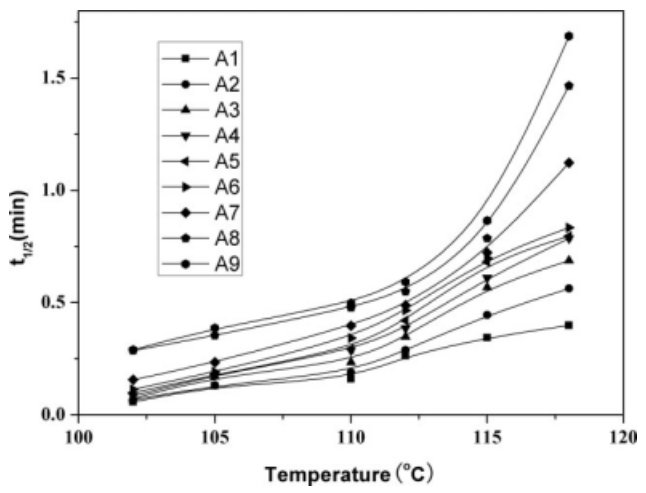

Figure 12 Effects of the HBPE content on the crystallization rate of the samples.

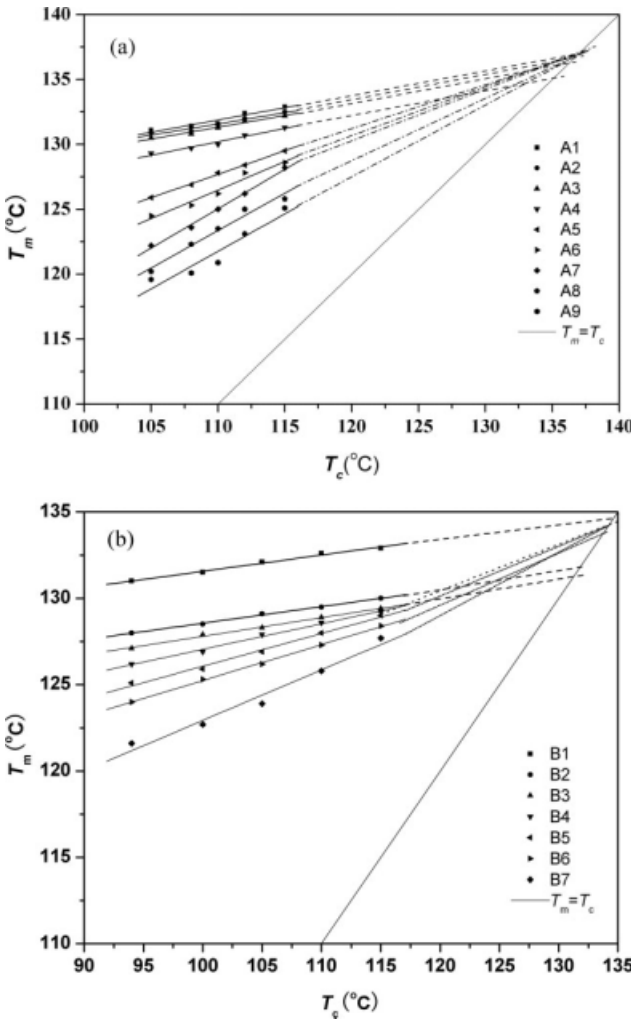

Figure 13 Plots of T_m versus T_c for the blends of sets A and B.

$$T_m^0 - T_m = \phi(T_m^0 - T_c) \quad (8)$$

where T_m^0 is the equilibrium melting point based on the Hoffman–Weeks approach and determined by the extrapolation of T_m versus T_c to $T_m = T_c$ and

TABLE IV
T_m^0 and ϕ Values for the Different Blend Compositions

	Sample									
	1	2	3	4	5	6	7	8	9	10
$W_{t\text{HBPE}}$ (%)[a]	0	13.8	17.9	28.5	42.8	54.8	71.0	78.7	90.5	100
T_m^0 (K)[a]	410.3	409.9	409.4	408.3	410.3	410.3	410.3	410.3	410.3	—[c]
ϕ[a]	0.06	0.19	0.19	0.20	0.35	0.40	0.09	0.49	0.50	—[c]
$W_{t\text{HBPE}}$ (%)[b]	0	14.9	22.1	34.5	44.1	61.2	74.9	100	—[d]	—
T_m^0 (K)[b]	408.1	404.9	404.4	408.1	408.1	408.1	408.1	—[c]	—	—
ϕ[b]	0.11	0.16	0.19	0.21	0.24	0.27	0.33	—[c]	—	—

[a] Parameter for set A.
[b] Parameter for set B.
[c] There were no T_m^0 or ϕ values for amorphous PEs A10 and B8.
[d] There were only eight samples in set B (i.e., no sample 9 or 10).

ϕ is the stability parameter depending on the crystalline thickness. T_m of the blends was much lower than T_m of the pure crystallizable content in evidence, and this indicates that such blends may be miscible.

The chemical potential of a polymer will be reduced by the addition of a miscible diluent because of thermodynamic considerations, and its decrease will lead to a decreasing value of T_m^0 if the polymer is crystallizable. Figure 13(a,b) shows plots of T_m versus T_c for the samples, revealing nearly linear correlations between T_m and T_c for all the samples. The traces of samples A1–A4 ($W_{t\text{HBPE}} \leq 28.5\%$) and B1–B3 ($W_{t\text{HBPE}} \leq 22.1\%$) are almost parallel. Table IV summarizes the T_m^0 values for all the samples obtained by the fitting of the data shown in Figure 13. It is noteworthy that the ϕ values were between 0 and 1: $\phi = 1$ suggests $T_m = T_c$ with inherently unstable crystals, whereas $\phi = 0$ implies $T_m = T_m^0$ with the most stable crystals. Obviously, the values of ϕ for samples A1–A4 were about 0.20 times less than those of samples A5–A9, and the values of ϕ for samples B1–B3 were less than 0.20; this indicates that the blends with lower amorphous contents were much more stable. However, the slopes of traces of T_m versus T_c for samples A5–A9 and B4–B7 with higher HBPE contents are different. These traces intersect with the trace of $T_m = T_c$ at the adjacent points higher than the parallel traces. The ϕ values of A8 and A9 were about 0.50, indicating lower stability, whereas B4–B7 still showed higher stability with ϕ values ranging from 0.2 to 0.33 because of the near thickness of the crystalline lamellae with the LPE B1. In other words, the thermodynamic factor played a vital role in the decrease in T_m when $W_{t\text{HBPE}}$ was relatively low (for set A, $W_{t\text{HBPE}} \leq 28.5\%$; for set B, $W_{t\text{HBPE}} \leq 22.1\%$), whereas the decrease in T_m for other samples was greatly determined by the dynamic variation of the thickness of the crystalline lamellae.

CONCLUSIONS

Two series of reactor blends of LPEs with low MWs and HBPEs with high MWs were successfully produced via a one-step, bicatalytic polymerization process. Set A consisted of reactor blends with LPE and less highly branched but higher MW PEs, and set B was composed of LPE and more highly branched but lower MW PEs. The microstructural characterization of these resins indicated that they were bimodal PEs, and the ratio of catalyst **1** to catalyst **2** or **3** dominated the MW and MWD of the resins. The analyses of the results obtained by DSC, WAXD, and SAXS indicated that the values of T_m, T_c, and X_C of these samples decreased with the increasing content of HBPE. However, the addition of HBPE did not disturb the crystallization process of LPE, even with much more highly branched and higher MW PEs, in comparison with the blends that we previously studied. In addition, the L_B values were greatly influenced by the concentration of HBPE and the branching degree. Therefore, they showed a slightly increasing tendency followed by a reduction. Cocrystallization and rearrangement of the crystalline lamellae occurred when the HBPE content was over 42.8% for blends of set A and over 61.2% for blends of set B; this indicated that the branching degree hindered the cocrystallization.

The isothermal analyses indicated that a lower amount of HBPE (for set A, $W_{t\text{HBPE}} \leq 28.5\%$; for set B, $W_{t\text{HBPE}} \leq 22.1\%$) added to the crystalline component acted as a diluent, whereas more HBPE always led to deformation or a reduction of the thickness of the lamellar crystallinity. At higher temperatures and higher HBPE contents, the crystallization rate decreased faster.

References

1. Soares, J. B. P.; Kim, J. D. J Polym Sci Part A: Polym Chem 2000, 38, 1408.
2. Soares, J. B. P.; Kim, J. D. J Polym Sci Part A: Polym Chem 2000, 38, 1427.
3. De Souza, R. F.; Casagrande, O. L., Jr. Macromol Rapid Commun 2001, 22, 1293.
4. Shan, C. L. P.; Soares, J. B. P.; Penlidis, A. Polymer 2002, 43, 7345.

5. Pan, L.; Zhang, K. Y.; Li, Y. G.; Bo, S. Q.; Li, Y. S. J Appl Polym Sci 2007, 104, 4188.
6. (a) Crowther, D. J.; Szul, J. F. U.S. Pat. 0,132,933 A1 (2004); (b) Cann, K. J.; Zhang, M. H.; Moorhouse, J. H.; Apecetche, M. A. U.S. Pat. 0,167,015 A1 (2004); (c) Kuo, C. I.; McCullough, L. G.; Shirodkar, P. P.; Ehrman, F. D.; Shannon, P. C.; Santana, R. L.; Ackerman, S. K.; O'Neil, D. G. U.S. Pat. 0,038,210 A1 (2005); (d) Kwalk, T. H. U.S. Pat. 0,036,041 A1 (2006); (e) Kwalk, T. H. U.S. Pat. 0,178,482 A1 (2006); (f) Jaker, S. U.S. Pat. 0,281,867 A1 (2006).
7. Martin, J. L.; Thorn, M. G.; McDaniel, M. P.; Jensen, M. D.; Yang, Q.; DesLauriers, P. J.; Kertok, M. E. U.S. Pat. 0,043,176 A1 (2007).
8. Chandrashekar, V.; Mack, M. P.; Gates, C. H., Jr.; Holland, C. S.; Nagy, N.; Nagy, S. M.; Vargas, E. S.; Merrick-Mack, J. A. U.S. Pat. 0,055,021 A1 (2007).
9. (a) Olivier, L.; Laurent, G.; Abbas, R. Int. Pat. WO 030,818 A2 (2005); (b) Eric, D. Int. Pat. WO 080,457 A1 (2005).
10. Wei, X.; Syriac, J. P.; Atieh, A.; Maneet, M.; Bing, W.; Nicolaas Hendrika, F. Int. Pat. WO 020,077 A1 (2007).
11. D'agnillo, L.; Soares, J. B. P.; Penlidis, A. J Polym Sci Part A: Polym Chem 1998, 36, 831.
12. Beigzadeh, D.; Soares, J. B. P.; Hamielec, A. H. J Appl Polym Sci 1999, 71, 1753.
13. Shan, C. L. P.; Soares, J. B. P.; Penlidis, A. Polymer 2003, 44, 177.
14. Beigzadeh, D.; Soares, J. B. P.; Duever, T. A. Macromol Rapid Commun 1999, 20, 541.
15. Kunrath, F. A.; Souza, R. F. D.; Casagrande, O. L., Jr. Macromol Rapid Commun 2000, 21, 277.
16. Mecking, S. Macromol Rapid Commun 1999, 20, 139.
17. Mota, F. F.; dos Santos, R. M.; de Souza, R. F.; Casagrande, O. L., Jr. Macromol Chem Phys 2001, 202, 1016.
18. Alobaidi, F.; Zhu, S. P. J Appl Polym Sci 2005, 96, 2212.
19. Alt, F. P.; Böhm, L. L.; Enderle, H. F.; Berthold, J. Macromol Symp 2001, 163, 135.
20. Mieda, N.; Yamaguchi, M. Adv Polym Technol 2007, 26, 173.
21. Hussein, I. A. Polym Int 2004, 53, 1327.
22. Liu, H. T.; Davey, C. R.; Shirodkar, P. P. Macromol Symp 2003, 195, 309.
23. Ahlers, A.; Kaminsky, W. Makromol Chem Rapid Commun 1988, 9, 457.
24. Heiland, K. W.; Kaminsky, W. Makromol Chem 1992, 193, 601.
25. Soares, J. B. P.; Kim, J. D. J Polym Sci Part A: Polym Chem 2000, 38, 1417.
26. Soares, J. B. P.; Read, D. J. Macromolecules 2003, 36, 10037.
27. Wu, T.; Li, Y.; Wu, G. Polymer 2005, 46, 3472.
28. Galante, M. J.; Mandelkern, L.; Alamo, R. G. Polymer 1998, 39, 5105.
29. Small, B. L.; Brookhart, M.; Bennett, A. M. A. J Am Chem Soc 1998, 120, 4049.
30. Liu, J. Y.; Zheng, Y.; Hu, N. H.; Li, Y. S. Chin J Chem 2006, 24, 1447.
31. Johnson, L. K.; Killian, C. M.; Brookhart, M. J Am Chem Soc 1995, 117, 6414.
32. Gates, D. P.; Svejda, S. A.; Oñate, E.; Killian, C. M.; Johnson, L. K.; White, P. S.; Brookhart, M. Macromolecules 2000, 33, 2320.
33. Ittel, S. D.; Johnston, L. K.; Brookhart, M. Chem Rev 2000, 100, 1169.
34. Zou, H.; Zhu, F. M.; Wu, Q.; Ai, J. Y.; Lin, S. A. J Polym Sci Part A: Polym Chem 2005, 43, 1325.
35. Jenkins, J. C.; Brookhart, M. J Am Chem Soc 2004, 126, 5827.
36. Michalak, A.; Ziegler, T. Macromolecules 2003, 36, 928.
37. Yin, J. H.; Mo, Z. S. Modern Polymer Physics (in Chinese); Science: Beijing, 2001.
38. Qiujada, R.; Dupont, J.; Correa, D. Macromol Rapid Commun 1995, 16, 357.
39. Soga, K.; Uozumi, T. Makromol Chem 1992, 193, 823.
40. Gallend, G. B.; de Souza, R. F.; Mauler, R. S.; Nunes, F. F. Macromolecules 1999, 32, 1620.
41. Zhao, Y.; Liu, S. S.; Yang, D. C. Macromol Chem Phys 1997, 198, 1427.
42. Arnal, M. L.; Cañizales, E.; Müller, A. J. Polym Eng Sci 2002, 42, 2048.
43. Yhe, J. T.; Chang, S. S.; Wu, T. W. J Appl Polym Sci 2008, 107, 854.
44. Krumme, A.; Lehtinen, A.; Adamovsky, S.; Sshick, C.; Roots, J.; Viikna, A. J Polym Sci Part B: Polym Phys 2008, 46, 1577.
45. Tanem, B. S.; Stori, A. Polymer 2001, 42, 5389.
46. Wang, Z. G.; Hsiao, B. S.; Sirota, E. B.; Srinivas, S. Polymer 2000, 41, 8825.
47. Chiu, H. J.; Chen, H. L. Polymer 2001, 42, 5749.